Directional support value of Gaussian transformation for infrared small target detection

Changcai Yang,[1] Jiayi Ma,[2,*] Shengxiang Qi,[3] Jinwen Tian,[3] Sheng Zheng,[4] and Xin Tian[2]

[1]College of Computer and Information Sciences, Fujian Agriculture and Forestry University, Fuzhou 350002, China

[2]Electronic Information School, Wuhan University, Wuhan 430072, China

[3]School of Automation, Huazhong University of Science and Technology, Wuhan 430074, China

[4]Institute of Intelligent Vision and Image Information, College of Science, China Three Gorges University, Yichang 443002, China

*Corresponding author: jyma2010@gmail.com

Received 15 September 2014; revised 5 February 2015; accepted 5 February 2015; posted 5 February 2015 (Doc. ID 223079); published 13 March 2015

Robust small target detection is one of the key techniques in IR search and tracking systems for self-defense or attacks. In this paper we present a robust solution for small target detection in a single IR image. The key ideas of the proposed method are to use the directional support value of Gaussian transform (DSVoGT) to enhance the targets, and use the multiscale representation provided by DSVoGT to reduce the false alarm rate. The original image is decomposed into sub-bands in different orientations by convolving the image with the directional support value filters, which are deduced from the weighted mapped least-squares–support vector machines (LS–SVMs). Based on the sub-band images, a support value of Gaussian matrix is constructed, and the trace of this matrix is then defined as the target measure. The corresponding multiscale correlations of the target measures are computed for enhancing target signal while suppressing the background clutter. We demonstrate the advantages of the proposed method on real IR images and compare the results against those obtained from standard detection approaches, including the top-hat filter, max–mean filter, max–median filter, min–local–Laplacian of Gaussian (LoG) filter, as well as LS–SVM. The experimental results on various cluttered background images show that the proposed method outperforms other detectors.

OCIS codes: (040.3060) Infrared; (100.2000) Digital image processing; (100.4999) Pattern recognition, target tracking.

http://dx.doi.org/10.1364/AO.54.002255

1. Introduction

The robust detection of IR small targets in clutter is one of the key techniques in IR search-and-track applications for self-defense or attacks [1–3]. Because the target is at a far distance, its projected image is usually very small and does not have adequate structure information for detecting or matching [4–7]. Moreover, the obtained IR small targets are often buried in a complex background with low signal-to-clutter ratio (SCR) due to the effects of inherent sensor noise or environment. Therefore, it is difficult to detect the small targets in complex IR background.

The classical small target detection methods, such as morphological top-hat filtering [1] or max–mean/max–median filter [2], focused on suppressing the background clutter or enhancing the small target. Based on morphological top-hat filtering, some new related methods have been presented [3,8–10]. The morphological top-hat filtering parameters are optimized by using neural network and genetic algorithm [3]. A judging value which is calculated following the properties of target region is imported into

1559-128X/15/092255-11$15.00/0

the top-hat transformation to enhance small target [8]. A new top-hat transformation method has been proposed [9], in which the classical top-hat transformation is reorganized by using two different but correlated structuring elements and the different information between the target and surrounding regions is taken into account. However, they sometimes do not give truly satisfactory results. The main difficulty is that the size of the small target may vary from 2 pixels × 2 pixels to 12 pixels × 12 pixels [11].

Many methods have been proposed to solve the scale problem. According to the principle of human discrimination of small targets from a natural scene, an efficient method using template matching based on the average gray absolute difference maximum map for the multiscale small target detection was proposed by Wang *et al.* [12]. A small targets detection method based on support vector machines (SVMs) in the wavelet domain was introduced by Wang *et al.* [13]. The fractal dimension algorithm based on wavelet transformation has been proposed to fuse mid-wave and long-wave IR images and detect targets [14]. Motivated by the robust properties of the human visual system (HVS), tune–max of the SCR-based scale-invariant small target detection has been proposed to solve the scale and clutter suppression problem [11].

Recently, a new method based on the least-squares–support vector machine (LS–SVM) has been proposed for small target detection [15]. This method applied LS–SVM model to generate a row and a column directional highpass template filters, and extracted the small target from the filtered images computed by filtering the original IR image with the two templates. Vasquez *et al.* [16] modeled the background as a collection of affine or quadratic trends. They proposed an efficient algorithm to segment the image into areas and estimate the linear parameter of the trend inside each area. The spatial bilateral filter (BF) is integrated with temporal profile to predict background without targets [17]. The concept of self-information is utilized to predict the gray value of a pixel in the background and the adaptive threshold method followed by a region growing technique is adopted to detect small targets [18]. Genin *et al.* [19] proposed a two-step scheme for point target detection method based on first- and second-order modeling of local background statistics. A background suppression method based on the nonlocal denoising filters principle is followed by a matched filter based on an estimate of the local spatial covariance matrix. Bae *et al.* [20] introduced an edge directional 2D least-mean squares (LMS) filter to predict the background excluding small targets. Small targets can be extracted by subtracting the predicted background from the original IR image. A new technique based on second-order directional derivative filter (SODD) and phase spectrum of Fourier transform (PFT) is proposed for small target detection [21]. Gao *et al.* [22] proposed an IR patchimage (IPI) model based on the nonlocal self-correlation property of the IR image for small target detection. Inspired by the contrast mechanism of human vision system and derived kernel model, a local contrast method for small IR target detection has been presented in [23]. These methods can usually achieve good performance in application but may become less effective for the small target in complex background.

In this paper, we explore a new robust IR small target detector that is more suitable for different clutter, noisy backgrounds, and target types. The contributions of this paper can be summarized as follows. First, we describe a directional support value of Gaussian transform (DSVoGT) approach for the multiscale representation of the IR image. Second, we propose a robust small target detection method, which uses the trace of the support value of Gaussian matrix from the IR image scale space.

2. Directional Support Value Filter

In this section, we first describe the necessary algorithm on which we based. Then we deduce the directional support value filter from the weighted mapped LS–SVM.

A. Mapped LS–SVM and Support Value Filter

Let $\mathbf{x} \in \mathbf{R}^d, \mathbf{y} \in \mathbf{R}, \mathbf{R}^d$ represents the input space, and d is its dimension. By some nonlinear feature mapping $\phi(\mathbf{x}):\mathbf{R}^d \to \mathbf{R}^q$, $\mathbf{x}$ is mapped into some a prior chosen Hilbert space spanned by the linear combination of a set of functions, where q denotes the dimension of the feature space. The aim of SVM is to estimate the function based on training data $\{(\mathbf{x}_i, \mathbf{y}_i)\}_{i=1}^N$. In LS–SVM [24,25], the basic approximation problem could be solved by a combination of a set of support vectors

$$f(\mathbf{x}) = \sum_{i=1}^{N} \alpha_i K(\mathbf{x}, \mathbf{x}_i) + b, \tag{1}$$

where α is the support value of support vector $\mathbf{x}_i$, and $K(\mathbf{x}, \mathbf{x}_i) = \phi(\mathbf{x})^T \phi(\mathbf{x}_i)$, $i = 1, \ldots, N$ is the kernel function satisfying the Mercer's condition.

The conditions for optimality can be written as the solution to the following set of linear equations

$$\begin{bmatrix} 0 & \vec{1}^T \\ \vec{1} & \Omega \end{bmatrix} \begin{bmatrix} b \\ \alpha \end{bmatrix} = \begin{bmatrix} 0 \\ \mathbf{Y} \end{bmatrix}, \tag{2}$$

where $\Omega = \mathbf{K} + \mathbf{I}/\gamma$, $\mathbf{K}_{ij} = K(\mathbf{x}_i, \mathbf{x}_j)$, $\mathbf{Y} = [y_1, \ldots, y_N]^T$, $\vec{1} = [1, \ldots, 1]^T$, and $\alpha = [\alpha_1, \ldots, \alpha_N]^T$. The parameter γ is a positive regularization constant.

In the 2D mapped LS–SVM [26], the LS–SVM is used to estimate the underlying intensity surface of an image. In this case, the input vector of the LS–SVM is defined by the pixel coordinate (r, c) and the output is the intensity value $g(r, c)$. Similar to the standard LS–SVM, the solution of the mapped LS–SVM is to solve a set of linear Eq. (2). The explicit solution of Eq. (2) can be given by

$$b = \frac{\vec{1}^T \Omega^{-1} \mathbf{Y}}{\vec{1}^T \Omega^{-1} \vec{1}}, \qquad \alpha = \Omega^{-1}(\mathbf{Y} - b\vec{1}). \tag{3}$$

In mapping LS–SVM [27,28], the input vectors $\{x_i, i = 1, \ldots, N\}$ are unchanged, and the parameters of the LS–SVM (kernel function K and parameter γ) can be priorly chosen, and elements of the vector $\mathbf{Y} = [g_1, \ldots, g_N]^T$ are taken from the $(2m+1) \times (2n+1)$ observed image intensity value matrix. Therefore, the Ω can be transformed into a constant matrix.

It is worth noting that Eq. (3) can be rewritten as follows

$$\alpha = \Omega^{-1}\left[\mathbf{I} - \vec{1}\left(\frac{\vec{1}^T \Omega^{-1}}{\vec{1}^T \Omega^{-1} \vec{1}}\right)^T\right]\mathbf{Y} = \mathbf{Q}\mathbf{Y}, \tag{4}$$

where $\mathbf{Q}$ is an $N \times N$ matrix defined by $\Omega^{-1}[\mathbf{I} - \vec{1}(\vec{1}^T \Omega^{-1}/\vec{1}^T \Omega^{-1}\vec{1})^T]$. For the observed pixel g_i in mapped neighborhood, the corresponding support value can be computed individually as a linear combination of the measured intensity values $\{g_i, i = 1, \ldots, N\}$. The weight associated with each is determined by the elements of the ith row vector of Matrix $\mathbf{Q}$. For a rectangular neighborhood, reshaping the corresponding row vector of Matrix $\mathbf{Q}$, the weight kernels become the support value filters. If the support value of the discrete image in the pixel (r, c) is approximated by the corresponding support value of the input vector defined at the mapped neighborhood center, the support values of the whole image can be computed by convolving the image with the support value filter deduced from the central row vector of Matrix $\mathbf{Q}$ [29].

B. Horizontal and Vertical Support Value Filters

To incorporate the prior information into LS–SVM, the weighted LS–SVM weights the error variables $e_k = \alpha_k / C$ with factors v_k [30]. In weighted LS–SVM, the linear Eq. (2) can be rewritten as

$$\begin{bmatrix} 0 & \vec{1}^T \\ \vec{1} & \Omega_C \end{bmatrix}\begin{bmatrix} b^* \\ \boldsymbol{\alpha}^* \end{bmatrix} = \begin{bmatrix} 0 \\ \mathbf{Y} \end{bmatrix}, \tag{5}$$

where $\Omega_C = \boldsymbol{K}(\mathbf{x}_i, \mathbf{x}_j) + \mathbf{V}_C$ and the diagonal matrix $\mathbf{V}_C$ is given by

$$\mathbf{V}_C = \mathrm{diag}\left\{\frac{1}{Cv_1}, \ldots, \frac{1}{Cv_N}\right\}. \tag{6}$$

Matrix $\mathbf{Q}$ can be rewritten as

$$\mathbf{Q}^* = \Omega_C^{-1}\left[\mathbf{I} - \vec{1}\left(\frac{\vec{1}^T \Omega_C^{-1}}{\vec{1}^T \Omega_C^{-1} \vec{1}}\right)^T\right]. \tag{7}$$

From Eqs. (5) and (7), we can see that $\mathbf{Q}^*$ depends on kernel function $\boldsymbol{K}$ and weighted function $\mathbf{V}_C$. One of the commonly used kernels is the Gaussian kernel, and this work focuses on the choice of the Gaussian radial basis function (RBF) kernel, $\boldsymbol{K}(\mathbf{x}, \mathbf{x}_i) = \exp(-\|\mathbf{x} - \mathbf{x}_i\|/2\sigma^2)$.

In order to enhance the definition of edges underlying image along the direction of the local edge, the solution is to adapt the shape of the neighborhood by giving each pixel different weight. One kind of weight function can be given by

$$v(r, c) = \frac{1}{\exp\left(-\frac{r_\theta^2}{2\sigma_r^2} - \frac{c_\theta^2}{2\sigma_c^2}\right)}, \tag{8}$$

where θ is the local edge orientation, and $\sigma_r \gg \sigma_c$, with $r_\theta = c \cos\theta + r \sin\theta$, $c_\theta = r \cos\theta - c \sin\theta$. The value of σ_c is chosen at least 3 times smaller than the average inter-edge distance.

Similar to the orthogonal wavelet transform, we set θ to be 0° and 90° for horizontal and vertical orientations, respectively. Then the horizontal and vertical support value filters $\boldsymbol{SVF}^h$ and $\boldsymbol{SVF}^v$ can be deduced from Eq. (7). The computation procedure of the direction support value filter can be summarized in Algorithm 1. If the spread parameter σ is set to be 0.6, C is set to be 1; σ_r and σ_c are set to be 40 and 0.5, respectively; and the size of the vector space is set to be 5 pixels × 5 pixels, the deduced horizontal support value filter is given as follows

$$\begin{bmatrix} -0.0000 & -0.0000 & -0.0000 & -0.0000 & -0.0000 \\ -0.0077 & -0.0166 & -0.0350 & -0.0166 & -0.0077 \\ -0.0255 & -0.1680 & 0.5548 & -0.1680 & -0.0255 \\ -0.0077 & -0.0166 & -0.0350 & -0.0166 & -0.0077 \\ -0.0000 & -0.0000 & -0.0000 & -0.0000 & -0.0000 \end{bmatrix}. \tag{9}$$

Algorithm 1. Computation procedure of the direction support value filter.

Input: Size of the mapped input vector space and parameters σ, C, θ, σ_r, and σ_c.
Output: Direction support value filter.
1. Calculate the $N \times N$ matrix Ω_C using $\boldsymbol{K}(\mathbf{x}_i, \mathbf{x}_j) + \mathbf{V}_C$.
2. Compute the $N \times N$ matrix $\mathbf{Q}$, where $Q = \Omega^{-1}[\mathbf{I} - \vec{1}(\vec{1}^T \Omega^{-1}/\vec{1}^T \Omega^{-1}\vec{1})^T]$.
3. Get the central row vector of Matrix $\mathbf{Q}$ and reshape it into a weight kernel and then obtain the direction support value filter.

3. DSVoGT-Based Small Target Detection

The directional support value filter can be extended to detect small targets. In the following we construct a support value of Gaussian matrix and then define the small target measure using the trace of this matrix. Then we present each step of the proposed method.

A. Support Value of Gaussian Matrix

When we represent scenes, generally the sizes of small targets are changing. It can be advantageous to represent the images at several scales. Similar to the support value of Gaussian function [31], a series of directional support value of Gaussian images can be obtained from the convolution of a variable-scale Gaussian. In this way, we can decompose the original image I into sub-bands in horizontal, vertical, and diagonal orientations with the following method

$$
\begin{aligned}
&I_l = I * G(x,y,\sigma_l), \qquad S_l^h = \boldsymbol{SVF}^h * I_l,\\
&S_l^v = I_l - S_l^h, \qquad S_l^{vv} = \boldsymbol{SVF}^v * S_l^v,\\
&S_l^{vh} = \boldsymbol{SVF}^v * S_l^h, \qquad S_l^{hh} = S_l^h - S_l^{vh}, \quad l = 1,\ldots,L,
\end{aligned}
\tag{10}
$$

where l is the scale level; the asterisk represents convolution operation; S^{hh}, S^{vv}, and S^{vh} are the support values of the original image obtained by multiscale decomposition in horizontal, vertical, and diagonal orientations, respectively; and

$$
G(x,y,\sigma_l) = \frac{1}{2\pi\sigma_l^2} e^{-(x^2+y^2)/2\sigma_l^2}. \tag{11}
$$

Based on these directional sub-bands of image, the DSVoGT can be developed. Similar to the standard support value of Gaussian transform (SVoGT) [31], the DSVoGT is a multiresolution transform with frame elements indexed by scale and location parameters. In practice, $\boldsymbol{SVF}^h$ is equal to $(\boldsymbol{SVF}^v)^T$. Figure 1 shows the support value decomposition at scale 1 for IR image. Figure 1(a) is an IR image under sky clutter background. Figure 1(b) shows the 3D gray value distribution for Fig. 1(a). Support values with horizontal, vertical, and diagonal orientations are shown in Figs. 1(c)–1(e), respectively. The proposed DSVoGT gives a multiscale representation containing multiple support values of Gaussian images which signify every target whose size is adapted to the resolution of the filter at each scale and whose orientation is in horizontal, vertical, or diagonal direction.

To effectively utilize the local structural information in the directional support value of Gaussian images, we define a support value of Gaussian matrix for each location (x,y) at Scale l as follows

$$
\boldsymbol{M}_l(x,y) = \begin{bmatrix} S_l^{hh}(x,y) & S_l^{vh}(x,y) \\ S_l^{vh}(x,y) & S_l^{vv}(x,y) \end{bmatrix}, \quad l = 1,\ldots,L. \tag{12}
$$

This matrix describes the support value of a point with its local neighborhood. As the support values represent the salient features underlying the image at Scale Level l, as shown in Figs. 1(f) and 1(g), the eigenvalues (λ_1,λ_2) of the support values of Gaussian matrix represent two principal signal changes in the neighborhood of a point. For small target, the absolute value of the sum of the eigenvalues is large, as shown in Fig. 1(h). This property enables the extraction of small targets, where the signal change is significant in both orthogonal directions. Based on this principle, we define the small targets measure as the trace of the support value of Gaussian matrix

$$
\boldsymbol{TM}_l(x,y) = \sigma_l^2 |S_l^{hh}(x,y) + S_l^{vv}(x,y)|. \tag{13}
$$

Since the trace of the matrix is equal to the sum of its eigenvalues, $\boldsymbol{TM}_l(x,y)$ reaches a maximum for blob-like small targets in the image. As illustrated in Figs. 2(a)–2(d), the new measures effectively integrate the information of the small targets at different orientations. As shown in Fig. 2, there is an inherent adaptivity of the analysis to the target size and orientation since the support of the convolution filter increases with the scale of analysis. The defined small target measures computed from the first level integrate the significant values at those locations where pixel-sized significant features are present [Fig. 2(a)], and significant measure values in the detail images correspond more and more to significant features of increasing spatial dimension with decreasing of the resolution [Figs. 2(b)–2(d)]. However, it is very difficult to pick up the interest features from the analysis of any single. This is because relevant support values are embedded in nonspecified background support values. To overcome the limitation of data coming from a single support value image and to distinguish important support values from nonrelevant ones, we take advantage of the multiresolution representation provided by the DSVoGT. We notice that small targets are features of interest represented by a small number of support values which are large and correlated across scales. For example, from Figs. 2(a)–2(d), we see that where there are small targets, the local maxima in small targets measure planes tend to propagate across scales, while others are not. We therefore design a multiscale spatial filtering scheme that results in small targets measure values that have high values in the presence of a small target and characterize it unambiguously, whereas they have nonsignificant values for the background. To that goal, we compute small target measure correlation $C_L^{\mathrm{TM}}(x,y)$ which is defined at each location (x,y) by the direct spatial multiscale product of the small targets measures values at adjacent scales in the measure value representation

$$
C_L^{\mathrm{TM}}(x,y) = \prod_{l=1}^{L} TM_l(x,y), \tag{14}
$$

where L is the lowest level at which the correlation is computed. Figure 2(e) illustrates the small target measure correlations, where Level L is 4. To visually inspect $C_L^{\mathrm{TM}}(x,y)$, a correlation image $\hat{C}_L^{\mathrm{TM}}$ is computed by normalizing the $C_L^{\mathrm{TM}}(x,y)$. Figure 2(f) shows the correlation image $\hat{C}_4^{\mathrm{TM}}$.

We subsequently use the fact that the product of significant measure values across scales at the location (x,y) results in significant values of $C_L^{\mathrm{TM}}(x,y)$ only if the local maxima propagate down to the considered scales. Obviously, if the local maxima are not present at some intermediate scale, this will largely decrease the values of $C_L^{\mathrm{TM}}(x,y)$. As illustrated in Fig. 2(e), the multiscale product of the small targets measure values effectively enhance the spot small targets, while degrading the background. The key observation in this context is that the small targets measure values at large scales are significant only in the vicinity of an important feature while they are close to zero elsewhere. On the other hand, for a given feature, the small targets measure value of its

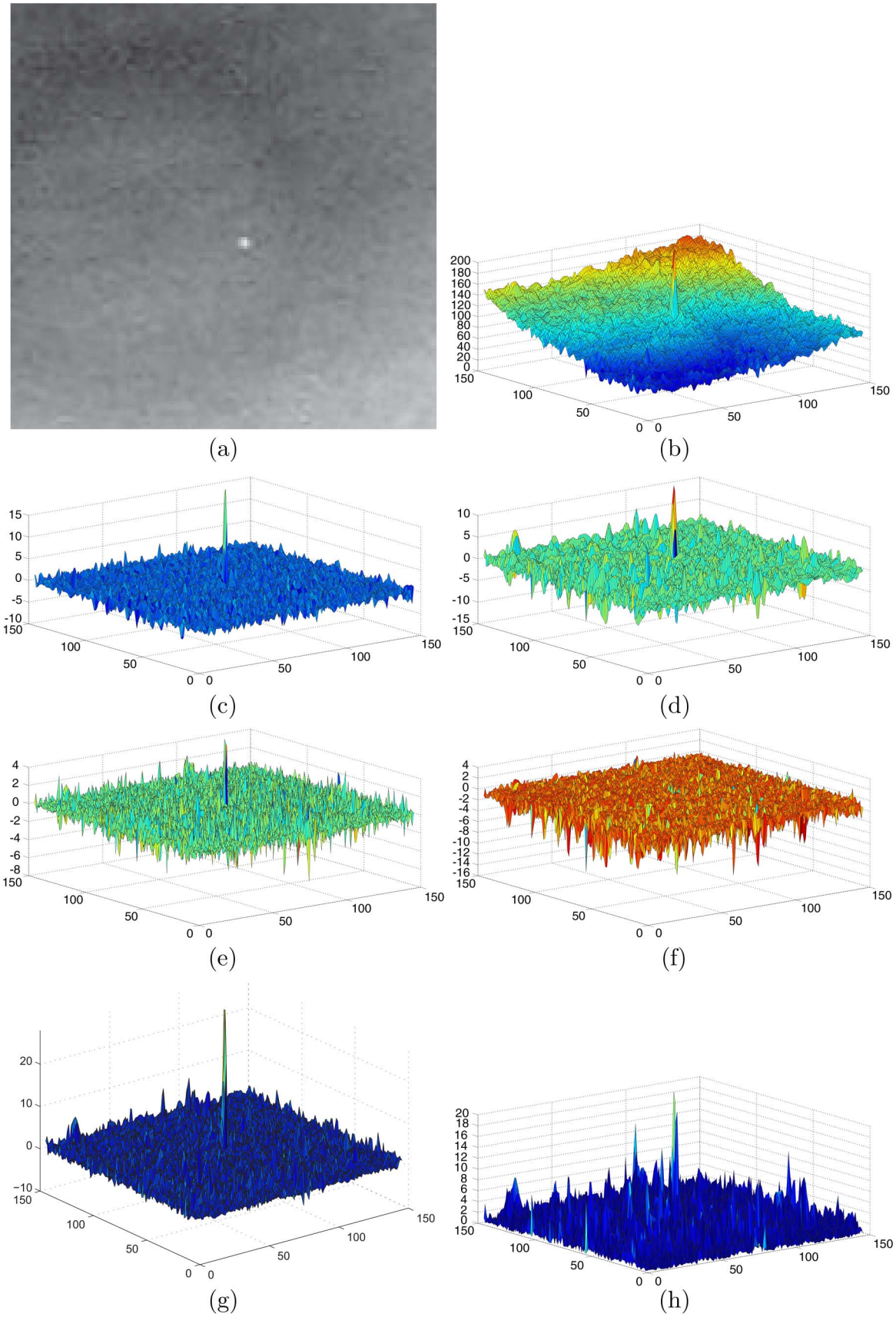

Fig. 1. Support value decomposition at Scale 1 for IR image; (a) original IR image under sky clutter background; (b) 3D gray value distribution of the original image; (c)–(e) support values with horizontal, vertical, and diagonal orientations, respectively; (f)–(g) eigenvalues of support value of Gaussian matrix; (h) absolute value of the sum of the eigenvalues.

interval of relevance decreases at small scales. The spatial filtering method can therefore be interpreted as a process by which support value images at large scales are used to give a coarse estimation of possible feature positions. This estimation is then refined by supplementing data coming from finer scales only at those spatially filtered locations. Therefore, the small targets measures deduced from the support value of Gaussian images effectively enhance the small targets underlying the image.

B. Small Target Detection Using DSVoGT

The correlation images can enhance the small targets and suppress the background clutter simultaneously as mentioned previously. Consequently, it is likely that $C_L^{\mathrm{TM}}(x,y)$ reach maxima for target in the scene. Based on this fact, an adaptive threshold is adopted to segment the small target

$$t_{\mathrm{th}} = \mu_{CI} + \tau\sigma_{CI}, \tag{15}$$

where μ_{CI} and σ_{CI} are the mean and the standard deviation of the correlation image, respectively; and τ is a constant determined experientially. A pixel at (x,y) is segmented as the target pixel if $C_L^{\mathrm{TM}}(x,y) > t_{\mathrm{th}}$, otherwise it is a background pixel. The detector, which can effectively extract the target in IR image, has a high detection rate and low false rate. In practice, τ

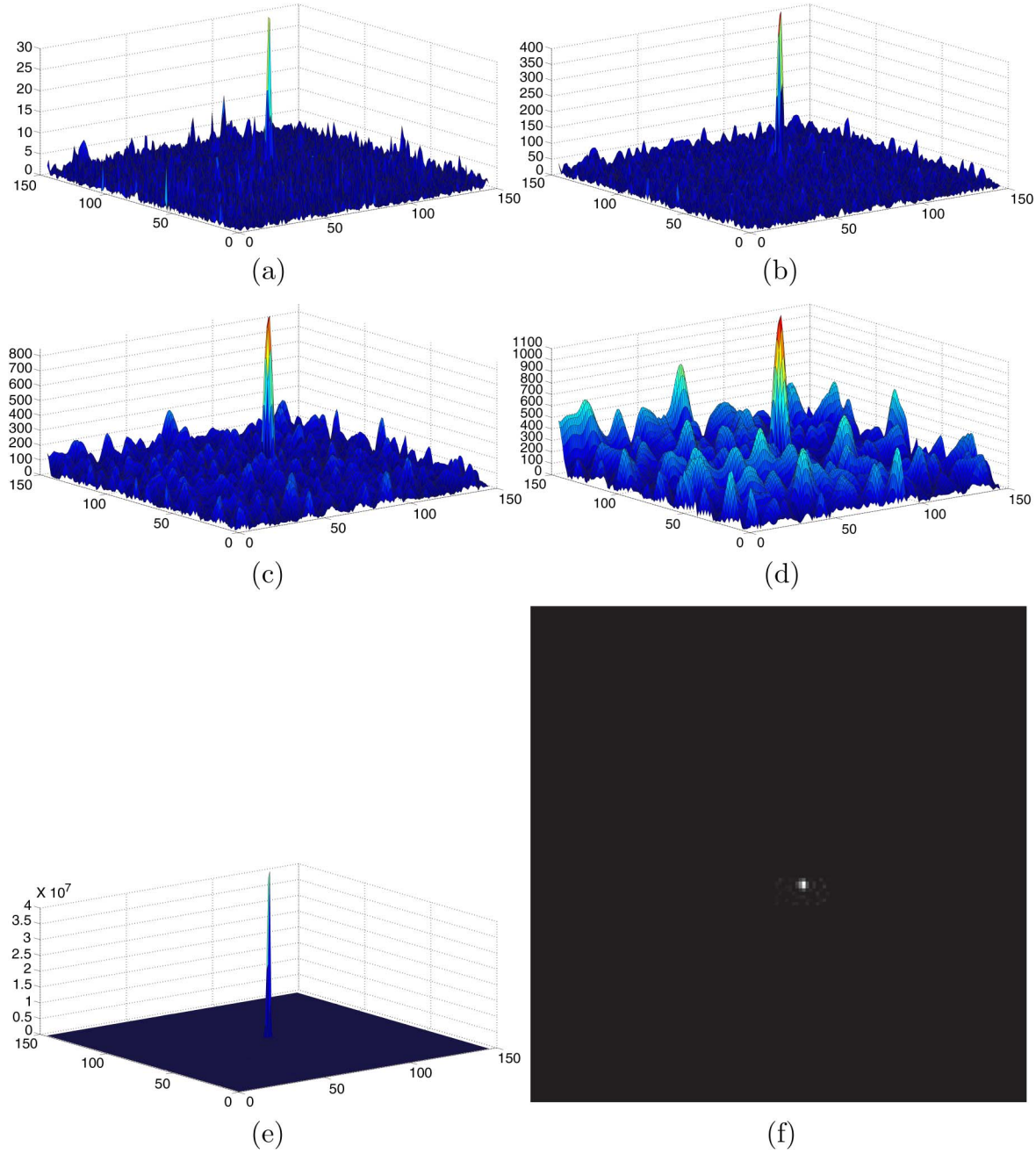

Fig. 2. Trace of the support value of Gaussian matrix correlations for IR image Fig. 1(a); (a)–(d) trace of the support value of Gaussian matrix at Scales 1–4, respectively; (e) small targets measure correlations C_4^{TM}; (f) correlation image $\hat{C}_4^{\mathrm{TM}}$.

usually ranges from 6 to 10. For the proposed DSVoGT method, the spread parameter σ_l for the Gaussian kernels $G(x,y,\sigma_l)$ in Eq. (10) is set to be $2^{\frac{l}{2}}(l=1,\ldots,4)$. The proposed DSVoGT based small target detection method is summarized in Algorithm 2, where the $\boldsymbol{SVF}^h$ in Eq. (9) is used.

Algorithm 2. DSVoGT-based small target detection method.

Input: IR image.
Output: Target regions.
1. Decompose the original image into sub-bands $\boldsymbol{S}_l^{hh}, \boldsymbol{S}_l^{vv}, \boldsymbol{S}_l^{vh}, l = 1,\cdots,L$ by Eq. (10).
2. Construct support value of Gaussian matrices $\boldsymbol{M}_l, l = 1,\cdots,L$ by Eq. (12).
3. Compute the trace support value of Gaussian matrices $\boldsymbol{TM}_l, l = 1,\cdots,L$ by Eq. (13).
4. Obtain the small target measure correlation C_L^{TM} by Eq. (14).
5. Compute the threshold t_{th} by Eq. (15).
6. Segment a pixel at (x,y) as the target pixel if $C_L^{\mathrm{TM}}(x,y) > t_{th}$, otherwise it is a background pixel.

4. Experiments and Discussion

In this section, we compare our method to other state-of-the-art approaches using the real IR images. The stability and accuracy of detectors are evaluated using the signal-to-clutter ratio gain (SCRG), background suppression factor (BSF), and receiver operation characteristic (ROC) curves. We also discuss the performance of different methods.

A. Experiment with Real Images

To evaluate the performance of the proposed method for small target detection, we test it on a set of collected real IR images. Those images are acquired using a scan-based long wave infrared (LWIR) camera. Column 1 in Fig. 3 is six representative images with various and complex clutters, such as uniform sky scene with a helicopter [Fig. 3(a)], cloud cluttered sky scene with an airplane [Fig. 3(b)], sea–sky scene with a ship [Figs. 3(c) and 3(d)], ground–sky scene with a car [Fig. 3(e)], and ground scene with a target [Fig. 3(f)]. The target sizes corresponding to Figs. 3(a)–3(f) are around 4×4, 3×5, 3×4, 6×7, 3×5, and 5×6, respectively. Figures 3(a)–3(f) are of sizes 146×146, 146×146, 276×224, 276×224, 216×136, and 316×252, respectively.

The proposed DSVoGT small target detector is compared to top-hat filter-based method [1], max–mean filter-based method [2], and max–median filter-based method [2] since these methods are well-studied and are usually used as baseline methods for assessing new methods [22,32]. Min–local–Laplacian

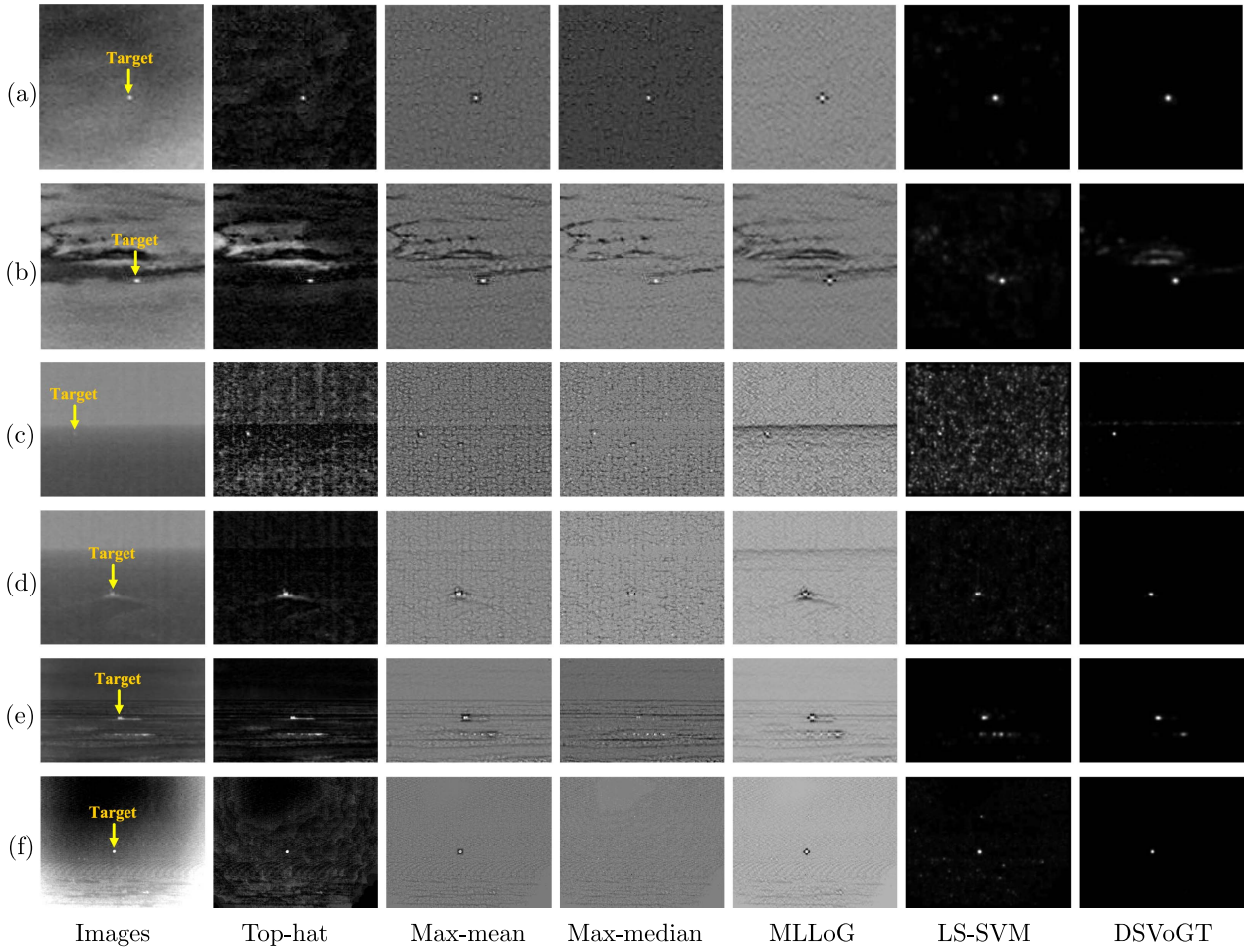

Fig. 3. Original images and the corresponding processed results of different methods.

of Gaussian (MLLoG) [33] and LS–SVM [15] methods are also chosen as the baseline methods. These detectors contain parameters that need to be adjusted in order to get the best performance for a specific application. In the experiments, the filter sizes of the top-hat, max–mean, max–median, MLLoG, and LS–SVM methods are set as 12×12, 9×9, 9×9, 1×15, and 15×15, respectively. Columns 2–7 in Fig. 3 show the processed results of six methods before segmentation. From Column 1 in Fig. 3(a), we can see that the target is small and is buried in the clutter sky background. For Fig. 3(a), top-hat method cannot well enhance the target region. And, there are still many clutter backgrounds remained surrounding the target region. The max–mean, max–median, and MLLoG methods can enhance the target region, but they could not suppress the clutter backgrounds which only make the intensities of backgrounds uniform, and hence could decrease the SCR. The LS–SVM and the proposed DSVoGT methods perform better than the top-hat, max–mean, max–median, and MLLoG methods. However, there are still some clutters around the target region in the result of LS–SVM. The proposed method suppresses almost all the clutter background. Similar results can be found in Figs. 3(b)–3(f). It can be seen that our method has less clutter and noise residual for different clutter backgrounds compared to the baseline methods, which is the key to keep lower P_f under the same P_d.

In the work, two common performance measures, SCRG and BSF, are used as standards for comparison which are defined as follows [34]

$$\mathrm{SCRG} = \frac{(S/C)_{\mathrm{out}}}{(S/C)_{\mathrm{in}}}, \qquad \mathrm{BSF} = \frac{C_{\mathrm{in}}}{C_{\mathrm{out}}}, \tag{16}$$

where S and C are the signal amplitude and clutter standard deviation; and in and out represent the input original image and the output target enhanced map, respectively. The same as the recent work [21], S is calculated as the difference between the mean values of targets and backgrounds, and C is calculated as the standard deviation of backgrounds.

Table 1 gives the values of quality of SCRG and BSF for the small target detection approaches. From Table 1, we can note that the proposed DSVoGT method provides the best target enhancement performance in terms of resulting values of SCRG. For Fig. 3(a), the SCRG value of the DSVoGT method is 67.74 and is greater than 6.40, 4.55, 0.17, 2.62, and 18.52, respectively, provided by the top-hat, max–mean, max–median, MLLoG, and LS–SVM methods. Similar results can be found for Figs. 3(b)–3(f). For Fig. 3(d), however, the SCRG value of the LS–SVM method is a little greater than the proposed DSVoGT method. From Table 1, we can note that the proposed DSVoGT method provides the best background clutter suppression performance in term of resulting value of BSF. The BSF value of the DSVoGT method is 90.16 and is greater than 3.90, 7.44, 7.74, 8.11, and 34.54, respectively, provided by the top-hat, max–mean, max–median, MLLoG, and LS–SVM methods. Similar results can be found for Figs. 3(b)–3(f).

In order to demonstrate the robustness of the proposed method, it is tested on the test images corrupted by Gaussian white noise of variance 0.0005 and 0.001. The SCRG and BSF values are given in Tables 2 and 3, respectively. We can find that the proposed method is robust to noise.

The ROC curve can also used to evaluate the performance of the small target detection methods. The ROC curve reflects the varying relationship between the detection probability P_d and the false alarm rate P_f which are defined as follows [35]

$$P_d = \frac{No.\,of\ \text{detected pixels}}{No.\,of\ \text{real target pixels}},$$
$$P_f = \frac{No.\,of\ \text{false alarms}}{\text{total pixels in the whole image}}. \tag{17}$$

Figure 4 shows the ROC curves of the six methods for six real IR images. The adaptive threshold in Eq. (15) is used to segment the target. The ROC curve of each method is obtained by changing τ in Eq. (15). Figure 4(a) shows the results for the uniform sky background from Fig. 3(a). The proposed method performs the best, followed by LS–SVM and max–median detectors. Figure 4(b) shows the results for the cloud cluttered sky background from Fig. 3(b). The method gives very low P_d scores, whereas the proposed method still provides sufficient P_d. Figures 4(c) and 4(d) show the results for the sea–sky background from Figs. 3(c) and 3(d). The proposed method performs the best, followed by LS–SVM and max–mean detectors. MLLoG and max–median detectors give low P_d. The worse results for MLLoG and max–median methods is due to that the gray

Table 1. SCRG and BSF Values of Different Methods for Each Test Image in Fig. 3

	Figure 3(a)		Figure 3(b)		Figure 3(c)		Figure 3(d)		Figure 3(e)		Figure 3(f)	
Images	SCRG	BSF	SCRG	BSF	SCRG	BSF	SCRG	BSF	SCRG	BSF	SCRG	BSF
Top-hat	6.40	3.90	4.47	2.65	13.13	0.93	1.42	0.88	1.28	0.69	12.84	2.62
Max–mean	4.55	7.44	2.95	4.02	9.89	1.20	1.65	1.77	0.80	0.97	4.33	2.38
Max–median	0.17	7.74	4.45	3.92	8.84	1.26	1.53	2.00	0.30	0.79	1.47	1.79
MLLoG	2.62	8.11	3.35	4.43	6.62	1.24	1.10	1.69	0.38	0.98	1.17	2.65
LS–SVM	18.52	34.54	24.55	40.26	12.61	2.27	**8.41**	12.72	3.29	6.07	9.29	11.47
DSVoGT	**67.74**	**90.16**	**31.66**	**61.68**	**139.88**	**26.52**	7.26	**14.39**	**4.34**	**6.55**	**74.55**	**38.05**

Table 2. SCRG and BSF Values of Different Methods on Various Test Images Corrupted by Gaussian White Noise of Variance 0.0005

	Figure 3(a)		Figure 3(b)		Figure 3(c)		Figure 3(d)		Figure 3(e)		Figure 3(f)	
Images	SCRG	BSF	SCRG	BSF	SCRG	BSF	SCRG	BSF	SCRG	BSF	SCRG	BSF
Top-hat	6.18	3.96	3.91	2.36	10.48	0.77	1.38	0.89	1.22	0.68	10.98	2.33
Max–mean	3.92	6.63	2.17	2.99	6.21	0.84	1.42	1.58	0.67	0.85	2.66	1.63
Max–median	0.47	7.50	2.96	2.87	4.54	0.93	1.46	1.79	0.18	0.65	0.84	1.08
MLLoG	2.57	7.64	2.94	3.83	6.13	1.17	1.13	1.71	0.36	0.92	1.04	2.38
LS–SVM	15.34	30.36	15.25	27.00	5.49	2.19	4.54	5.46	2.35	3.58	2.86	3.95
DSVoGT	**66.80**	**93.82**	**32.36**	**59.24**	**112.06**	**21.34**	**6.39**	**12.25**	**4.36**	**6.50**	**77.37**	**42.05**

Table 3. SCRG and BSF Values of Different Methods on Various Test Images Corrupted by Gaussian White Noise of Variance 0.001

	Figure 3(a)		Figure 3(b)		Figure 3(c)		Figure 3(d)		Figure 3(e)		Figure 3(f)	
Images	SCRG	BSF	SCRG	BSF	SCRG	BSF	SCRG	BSF	SCRG	BSF	SCRG	BSF
Top-hat	5.63	3.65	3.00	1.98	7.95	0.73	1.29	0.85	1.14	0.66	9.85	2.10
Max–mean	3.55	5.89	1.70	2.37	4.47	0.87	1.36	1.50	0.52	0.67	2.10	1.33
Max–median	0.53	6.71	2.48	2.32	3.31	0.95	1.26	1.53	0.20	0.50	0.98	0.99
MLLoG	2.40	7.09	2.79	3.42	5.51	1.11	1.12	1.66	0.37	0.96	1.07	2.19
LS–SVM	13.46	29.27	9.65	15.34	2.08	1.85	3.16	3.68	2.76	5.88	1.14	2.06
DSVoGT	**64.95**	**93.87**	**32.26**	**61.53**	**96.82**	**15.74**	**7.22**	**13.67**	**4.21**	**6.58**	**67.24**	**36.37**

intensity differences between the target and the background are not sufficient for MLLoG and max–median detectors to enhance the target from low SCR IR image. Figure 4(a) shows the results for the ground–sky background from Fig. 3(e). The proposed method performs the best, followed by LS–SVM, max–mean, and top-hat detectors. Figure 4(f) shows the results for the ground background from Fig. 3(f). The proposed method, LS–SVM, and top-hat perform the best, followed by max–mean.

In summary, the top-hat method obtains high P_d scores for the cases of the uniform sky background, sea–sky background, and ground background, but shows low performances for the case of the cloud-cluttered sky background. For most experiments the proposed method performs the best, followed by LS–SVM method. This demonstrates that the proposed method is robust and effective for different clutter and noisy backgrounds and target types.

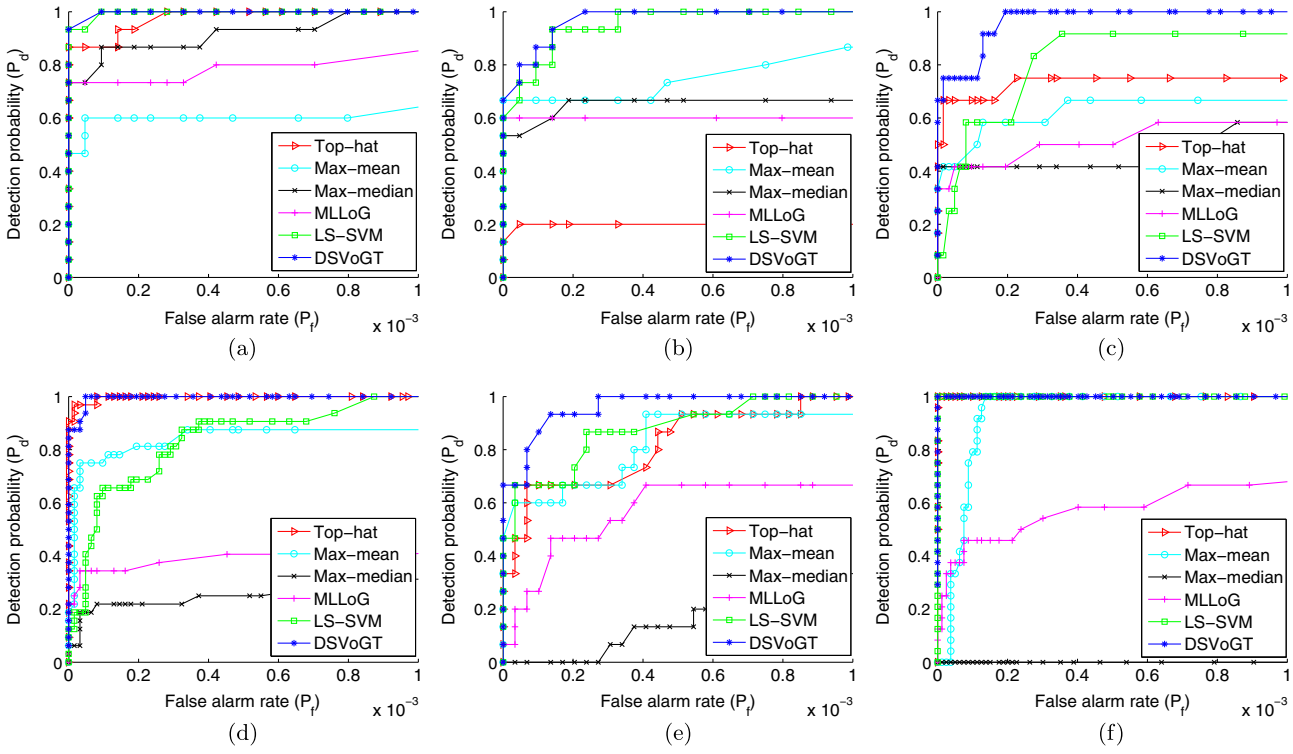

Fig. 4. ROC curves of six methods for each test image in Fig. 3.

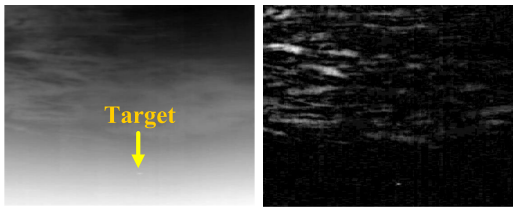

(a)Original image (b)Top-hat

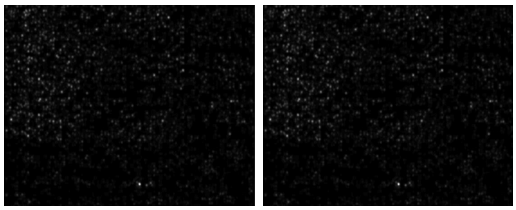

(c)LS-SVM (d)DSVoGT

Fig. 5. One frame in image sequence and the corresponding processed results of different methods; (a) original image; (b) top-hat; (c) LS–SVM; (d) DSVoGT.

B. Experiment with Image Sequence

In this section, we perform experiments on the sequence with heavily cloudy clutter background. The test sequence contains 117 frames, the image is of the size 448 × 557, and the target is an airplane. The top-hat and LS–SVM methods perform better than other baseline methods as mentioned previously. We compare our method to top-hat [1] and LS–SVM [15]. The ROC curve is again used as a standard for comparison. For the sequence, the detection probability P_d and the false alarm rate P_f are defined as follows

$$P_d = \frac{No.\,of \text{ correctly detected targets}}{No.\,of \text{ true targets}},$$
$$P_f = \frac{No.\,of \text{ incorrectly detected targets}}{No.\,of \text{ images}}. \quad (18)$$

The positions of the detected targets are compared to the ground truth. The targets are labeled as correctly detected targets if the correspondences with the ground truth (in this context, the pixel distance of their centers is within 5 pixels) is found and as incorrectly detected targets otherwise.

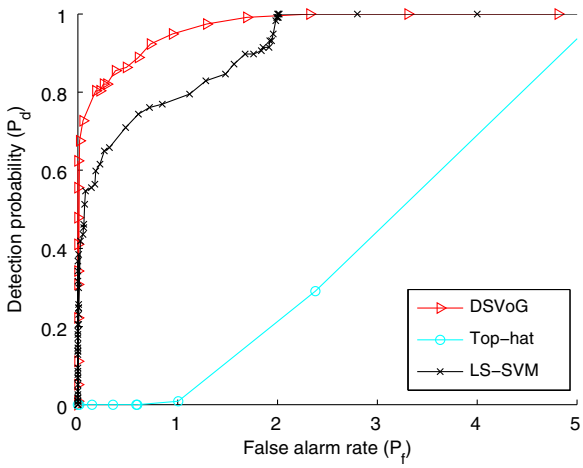

Fig. 6. ROC curves of sequence.

The processed results of one frame by different methods are shown in Fig. 5. As can be seen from Fig. 5, the DSVoGT method has less clutter and noise residual. Figure 6 shows the results of the three methods for real image sequence. Our approach performs the best, and it consistently outperforms the baseline methods.

5. Conclusions

In this paper, we develop the directional support value filters and the directional support value analysis method, and present DSVoGT-based small target detection method. We have carried out the performance comparison among the proposed DSVoGT, top-hat [1], max–mean [2], max–median [2], MLLoG [33], and LS–SVM [15]. The experimental results on real IR images show the performance of our approach. The trace of the support value of Gaussian matrix of the proposed DSVoGT method is effective to measure the small target even for low SCR images. The multi-scale products of the target measures effectively enhance the targets while suppress the background clutter, and demonstrate some advantages over other methods on detecting small targets.

This work was supported in part by the National Natural Science Fund Committee of the Chinese Academy of Sciences astronomical union funds under Grant U1331113, by the National Natural Science Foundation of China under Grant 61102064, and by the China Postdoctoral Science Foundation under Grants 2013M540582 and 2014T70702.

References

1. V. T. Tom, T. Peli, M. Leung, and J. E. Bondaryk, "Morphology-based algorithm for point target detection in infrared backgrounds," Proc. SPIE **1954**, 2–11 (1993).
2. S. D. Deshpande, M. H. Er, V. Ronda, and P. Chan, "Max-mean and max-median filters for detection of small targets," Proc. SPIE **3809**, 74–83 (1999).
3. M. Zeng, J. Li, and Z. Peng, "The design of top-hat morphological filter and application to infrared target detection," Infrared Phys. Technol. **48**, 67–76 (2006).
4. J. Ma, J. Zhao, J. Tian, A. L. Yuille, and Z. Tu, "Robust point matching via vector field consensus," IEEE Trans. Image Process. **23**, 1706–1721 (2014).
5. J. Ma, J. Zhao, J. Tian, Z. Tu, and A. L. Yuille, "Robust estimation of nonrigid transformation for point set registration," in *IEEE Conference on Computer Vision and Pattern Recognition* (IEEE, 2013), pp. 2147–2154.
6. J. Ma, J. Zhao, Y. Ma, and J. Tian, "Non-rigid visible and infrared face registration via regularized Gaussian fields criterion," Pattern Recogn. **48**, 772–784 (2015).
7. C. Yang, J. Ma, M. Zhang, S. Zheng, and X. Tian, "Multiscale facet model for infrared small target detection," Infrared Phys. Technol. **67**, 202–209 (2014).
8. X. Bai, F. Zhou, and T. Jin, "Enhancement of dim small target through modified top-hat transformation under the condition of heavy clutter," Signal Process. **90**, 1643–1654 (2010).
9. X. Bai and F. Zhou, "Analysis of new top-hat transformation and the application for infrared dim small target detection," Pattern Recogn. **43**, 2145–2156 (2010).

10. W. Meng, T. Jin, and X. Zhao, "Adaptive method of dim small object detection with heavy clutter," Appl. Opt. **52**, D64–D74 (2013).
11. S. Kim and J. Lee, "Scale invariant small target detection by optimizing signal-to-clutter ratio in heterogeneous background for infrared search and track," Pattern Recogn. **45**, 393–406 (2012).
12. G. Wang, T. Zhang, L. Wei, and N. Sang, "Efficient method for multiscale small target detection from a natural scene," Opt. Eng. **35**, 761–768 (1996).
13. Z. Wang, J. Tian, J. Liu, and S. Zheng, "Small infrared target fusion detection based on support vector machines in the wavelet domain," Opt. Eng. **45**, 076401 (2006).
14. Y. Sun, J. Tian, and J. Liu, "Novel method on dual-band infrared image fusion for dim small target detection," Opt. Eng. **46**, 116402 (2007).
15. P. Wang, J. Tian, and C. Gao, "Infrared small target detection using directional highpass filters based on LS-SVM," Electron. Lett. **45**, 156–158 (2009).
16. E. Vasquez, F. Galland, G. Delyon, and P. Réfrégier, "Mixed segmentation-detection-based technique for point target detection in nonhomogeneous sky," Appl. Opt. **49**, 1518–1527 (2010).
17. T. W. Bae, "Small target detection using bilateral filter and temporal cross product in infrared images," Infrared Phys. Technol. **54**, 403–411 (2011).
18. H. Deng and J. Liu, "Infrared small target detection based on the self-information map," Infrared Phys. Technol. **54**, 100–107 (2011).
19. L. Genin, F. Champagnat, and G. Le Besnerais, "Background first- and second-order modeling for point target detection," Appl. Opt. **51**, 7701–7713 (2012).
20. T. W. Bae, F. Zhang, and I. S. Kweon, "Edge directional 2D LMS filter for infrared small target detection," Infrared Phys. Technol. **55**, 137–145 (2012).
21. S. Qi, J. Ma, C. Tao, C. Yang, and J. Tian, "A robust directional saliency-based method for infrared small-target detection under various complex backgrounds," IEEE Geosci. Remote Sens. Lett. **10**, 495–499 (2013).
22. C. Gao, D. Meng, Y. Yang, Y. Wang, X. Zhou, and A. Hauptmann, "Patch-image model for small target detection in a single image," IEEE Trans. Image Process. **22**, 4996–5009 (2013).
23. C. Chen, H. Li, Y. Wei, T. Xia, and Y. Tang, "A local contrast method for small infrared target detection," IEEE Trans. Geosci. Remote Sens. **52**, 574–581 (2014).
24. J. A. K. Suykens and J. Vandewalle, "Least squares support vector machine classifiers," Neural Process. Lett. **9**, 293–300 (1999).
25. J. A. K. Suykens, T. V. Gestel, J. D. Brabanter, B. D. Moor, and J. Vandewalle, *Least Squares Support Vector Machines* (World Scientific, 2002).
26. S. Zheng, Y. Q. Sun, J. W. Tian, and J. Liu, "Mapped least squares support vector regression," Int. J. Patt. Recogn. Art. Intell. **19**, 459–475 (2005).
27. S. Zheng, W. Z. Shi, J. Liu, J. W. Tian, and G. X. Zhu, "Multi source image fusion method using support value transform," IEEE Trans. Image Process. **16**, 1831–1839 (2007).
28. S. Zheng, C. Yang, B. L. Kaptein, E. A. Hendriks, O. H. Koning, and B. Lei, "Support value based stent-graft marker detection," Pattern Recogn. **46**, 962–975 (2013).
29. C. Yang, S. Zheng, and J. Ye, "Level set contour extraction method based on support value filter," Appl. Math. Comput. **205**, 688–696 (2008).
30. J. A. Suykens, J. D. Brabanter, L. Lukas, and J. Vandewalle, "Weighted least squares support vector machines: robustness and sparse approximation," Neurocomputing **48**, 85–105 (2002).
31. C. Yang, C. Tao, Y. Fu, J. Tian, and Z. Sheng, "Support value of Gaussian-based interest point detector," Opt. Eng. **49**, 117006 (2010).
32. S. Qi, D. Ming, J. Ma, X. Sun, and J. Tian, "Robust method for infrared small target detection using Boolean map visual theory," Appl. Opt. **53**, 3929–3940 (2014).
33. S. Kim, "Min-local-log filter for detecting small targets in cluttered background," Electron. Lett. **45**, 105–106 (2011).
34. C. I. Hilliard, "Selection of a clutter rejection algorithm for real-time target detection from an airborne platform," Proc. SPIE **4048**, 74–84 (2000).
35. Y. Gu, C. Wang, B. Liu, and Y. Zhang, "A kernel based nonparametric regression method for clutter removal in infrared small-target detection applications," IEEE Geosci. Remote Sens. Lett. **7**, 469–473 (2010).